npj | parkinson's disease

Article

Published in partnership with the Parkinson's Foundation

https://doi.org/10.1038/s41531-025-00892-6

SVHRSP protects against rotenone-induced neurodegeneration in mice by inhibiting TLR4/NF-κB-mediated neuroinflammation via gut microbiota

Mengdi Chen[1,5], Yu Zhang[1,2,5], Liyan Hou[3,5], Zirui Zhao[1], Peiyan Tang[1], Qingquan Sun[1], Jie Zhao[1] ✉ & Qingshan Wang[1,4] ✉

Strong evidence indicates that remodeling gut microbiota may be an effective approach to combat Parkinson's disease (PD). Scorpion Venom Heat-Resistant Synthesized Peptide (SVHRSP), a synthesized peptide discovered from scorpion venom, displays potent neuroprotection in multiple PD models. However, the potential mechanisms remain unclear. In this study, we demonstrated that SVHRSP effectively attenuated gastrointestinal function impairments and reinstated the microbiota composition in rotenone-induced PD mouse model. Microbiota depletion and FMT verified that the restored gut microbiota was necessary for SVHRSP-mediated neuroprotection against dopaminergic neurodegeneration in rotenone PD mice. Furthermore, SVHRSP gut microbiota-dependently attenuated BBB impairment, microglial activation, and gene expression of pro-inflammatory factors in rotenone-treated mice. Mechanistically, SVHRSP decreased the concentrations of LPS and HMGB1 in both serum and brain tissue, thereby inhibiting the TLR4/NF-κB signaling pathway in the brain of rotenone-treated mice. Together, our findings provided fresh perspectives on the mechanisms underlying SVHRSP-induced neuroprotection in PD.

Parkinson's disease (PD) ranks as the second most prevalent neurodegenerative disease with its occurrence increasing year by year. PD is distinguished by the degeneration of dopaminergic neurons within the substantia nigra (SN) and the intraneuronal aggregation of α-synuclein[1]. The clinical features of PD include motor symptoms and non-motor symptoms[2]. Non-motor symptoms in PD usually appear prior to motor symptoms, such as olfactory dysfunction, constipation, and REM sleep behavioral disorder[3]. Currently, the treatment of PD mainly focuses on symptom relief and fails to halt the neurodegenerative process. Therefore, the development of innovative therapeutic strategies aimed at halting neurodegeneration is urgently needed.

Recent investigations have uncovered a strong link between gastrointestinal dysfunction and the onset and progression of PD. Fecal microbiota analyzed using 16S rRNA sequencing showed a significant reduction in bacterial taxa related to neuroprotection in PD patients compared to control individuals[4]. Further studies revealed a significant positive correlation between decreased Enterobacteriaceae and increased postural instability in PD patients[5]. Additionally, a negative association between PD severity/duration and cellulose-degrading microorganisms was observed[6]. Notably, when feces from PD patients were transplanted into mice, the neuropathological manifestations of PD, such as dopaminergic neurodegeneration and motor dysfunction were replicated[7]. Germ-free or microbiota-depleted mice showed more resistance to feces-induced neuropathological damage from PD patients than normal mice[8,9], indicating that microbiota dysbiosis contributes to the advancement of PD.

Disruptions in the bacterial microbiota have been shown to induce intestinal inflammation. Evidence from experiments, clinical observations, and population studies indicates that intestinal inflammation is one of the mechanisms underlying the development of PD[10,11]. PD patients show a notable rise in pro-inflammatory bacteria such as Lactobacillus, Akkermansia, Helicobacter, and Enterobacter in the intestinal mucosa compared with non-PD controls[12]. In contrast, PD patients have reduced levels of

[1]National-Local Joint Engineering Research Center for Drug-Research and Development (R&D) of Neurodegenerative Diseases, Dalian Medical University, Dalian, China. [2]Center of Genome and Personalized Medicine, Institute of Cancer Stem Cell, Dalian Medical University, Dalian, China. [3]Dalian Medical University Library, Dalian Medical University, Dalian, China. [4]School of Public Health, Dalian Medical University, Dalian, China. [5]These authors contributed equally: Mengdi Chen, Yu Zhang, Liyan Hou. ✉e-mail: zhaoj@dmu.edu.cn; wangq4@126.com

Roseburia bacteria, which can modulate genes associated with anti-inflammatory effects, compared to healthy individuals[13]. Heightened level of pro-inflammatory cytokines and glial markers has been observed in the colons of PD patients[14]. This pro-inflammatory dysbiosis evident in PD patients might lead to misfolding of α-synuclein and compromise the integrity of the intestinal barrier, ultimately leading to breakdown of the blood–brain barrier (BBB) and subsequent neuroinflammation and neurodegeneration in the brain[15,16]. Some studies have suggested that certain natural drugs may exert neuroprotective effects through modulation of the gut microbiota. For instance, curcumin-induced protection in PD mice was associated with the levels of Lactobacillaceae and Aerococcaceae[17]. Coffee improved gut microbiota dysbiosis induced by MPTP in a mouse model and this improvement was linked to a reduction of dopaminergic neurodegeneration in mice[18]. Therefore, reshaping the gut microbiota could be explored as an innovative direction for developing PD treatment strategies.

The Scorpion Venom Heat-Resistant Synthesized Peptide (SVHRSP), derived from the venom of East Asian scorpions, is obtained through a combination of liquid chromatography–mass spectrometry, solid-phase chemical synthesis, chromatographic purification, and mass spectrometry identification techniques by our laboratory. We have recently demonstrated that SVHRSP exhibits neuroprotective effects in various mouse models of PD[19,20]. However, the mechanisms underlying SVHRSP-afforded neuroprotection remain unclear. The study aimed to explore the impact and underlying mechanisms of SVHRSP on gut dysbiosis employing a rotenone-induced mouse PD model, aiming to provide a deeper insight into the mechanisms responsible for SVHRSP's neuroprotection.

Results

SVHRSP alleviates constipation behaviors in rotenone-induced PD mice

To assess the potential of SVHRSP in alleviating intestinal dysfunction in a rotenone (Rot)-induced PD mouse model, we assessed the defecation frequency, fecal water content, and intestinal motility among the groups. Rotenone-induced PD mice exhibited a notable decrease in defecation frequency and fecal water content when compared to the control mice (Fig. 1a, b). Notably, SVHRSP treatment significantly mitigated the decrease in defecation frequency and fecal water content induced by rotenone in mice (Fig. 1a, b). Additionally, the impaired intestinal transit distance in rotenone-induced PD mice was also alleviated by SVHRSP treatment (Fig. 1c). These results indicate that SVHRSP might alleviate rotenone-induced intestinal dysfunction.

SVHRSP attenuates fecal microbiota dysbiosis in rotenone-induced PD mice

The composition and abundance of bacteria have been noted to change in both PD patients and mouse models. To study the influence of SVHRSP on the intestinal microbiota, we performed 16S rRNA sequencing on fecal samples obtained from mice in different groups. Initially, alpha-diversity analysis was used to assess the richness and variety of bacterial species. As shown in Fig. 2a, c, we observed an elevated Shannon index and Simpson index in the rotenone-induced PD mice in comparison to the control mice. In contrast, compared with the rotenone-induced PD mice, the mice in the Rot + SVHRSP group displayed decreased values for both indices (Fig. 2a, b). Subsequently, beta diversity, determined using weighted UniFrac distances, was used to assess the consistency of microbiota composition among these three groups. The bacterial compositions of the control, rotenone, and Rot + SVHRSP groups were found to be significantly distinct (Fig. 2c).

To evaluate the impact of SVHRSP on the microbiome, a comparison of microbial groups was executed at the phylum level. Rotenone PD mice exhibited elevated Actinobacteria compared to the control mice, which was notably reduced by SVHRSP (Fig. 2d). Similarly, at the genus level, Allobaculum and Bifidobacterium showed elevated relative abundances in rotenone PD mice compared to the control mice. SVHRSP treatment reduced the rotenone-induced elevation of Allobaculum and Bifidobacterium in mice (Fig. 2e). We then identified the most significant differential amplicon sequence variants (ASVs) between Rot versus Con and Rot + SVHRSP versus Rot group. Subsequently, we identified the overlaps of the most highly differential ASVs between the Rot group versus Con group and the Rot + SVHRSP group versus Rot group (Fig. 2f), defining these taxa as SVHRSP-sensitive ASVs. Among these ASVs, ASV_6 annotated as g_Allobaculum and ASV_151 and ASV_11 annotated as g_Bifidobacterium were downregulated after SVHRSP treatment compared with the Rot group. In contrast, ASV_57 annotated as g_Desulfovibrio was upregulated after SVHRSP treatment. These findings imply that the microbiota could have a significant impact on alleviating intestinal dysfunction mediated by SVHRSP.

To elucidate alterations in the functional pathway of the gut microbiota, we conducted KEGG enrichment analysis. Significant pathways enriched between the Rot group versus Con group and the Rot + SVHRSP group versus Rot group were identified (Fig. 2g). Among these pathways, both the 'Superpathway of Glycerol Degradation to 1,3-Propanediol' and 'Mevalonate Pathway I' were involved in lipid synthesis, which have been indicated to have a role in PD and were inhibited after SVHRSP treatment compared with the Rot group. Additionally, the 'L-Glutamate Degradation VIII (to Propanoate)' pathway, associated with excitotoxicity of glutamate, was also inhibited following SVHRSP treatment compared to the Rot group. Taken together, these results suggested that the quantity and population of gut microbes in rotenone-induced PD mice were both restored after SVHRSP administration.

SVHRSP reverses abnormalities in metabolites of the microbiota in rotenone-induced PD mice

Metabolites serve as signal molecules and substrates for metabolic reactions within the intestinal microbiota. Changes in the population of gut microbes can result in modifications in metabolite profiles. To explore the correlation between SVHRSP and the gut microbiota, we performed a comparative analysis of fecal metabolic profiles among the groups using untargeted

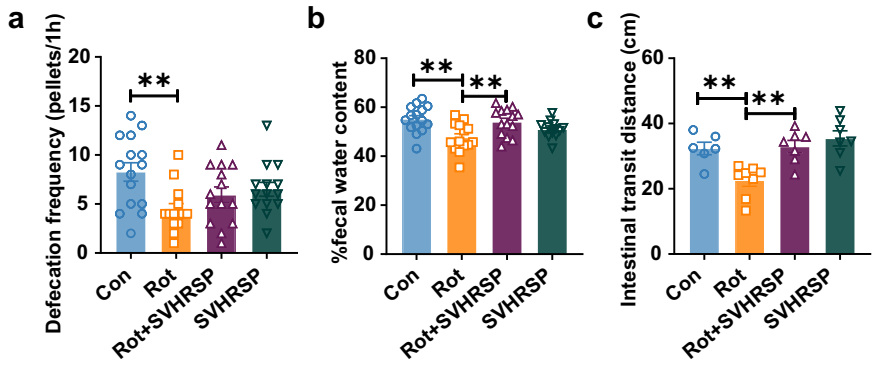

Fig. 1 | SVHRSP alleviates the constipation-like behaviors and intestinal motility in rotenone-induced PD mice. a The frequency of defecation. **b** Fecal water content. $n = 14–15$. **c** The intestinal transit distance of mice. $n = 6–8$. $^{**}p < 0.01$.

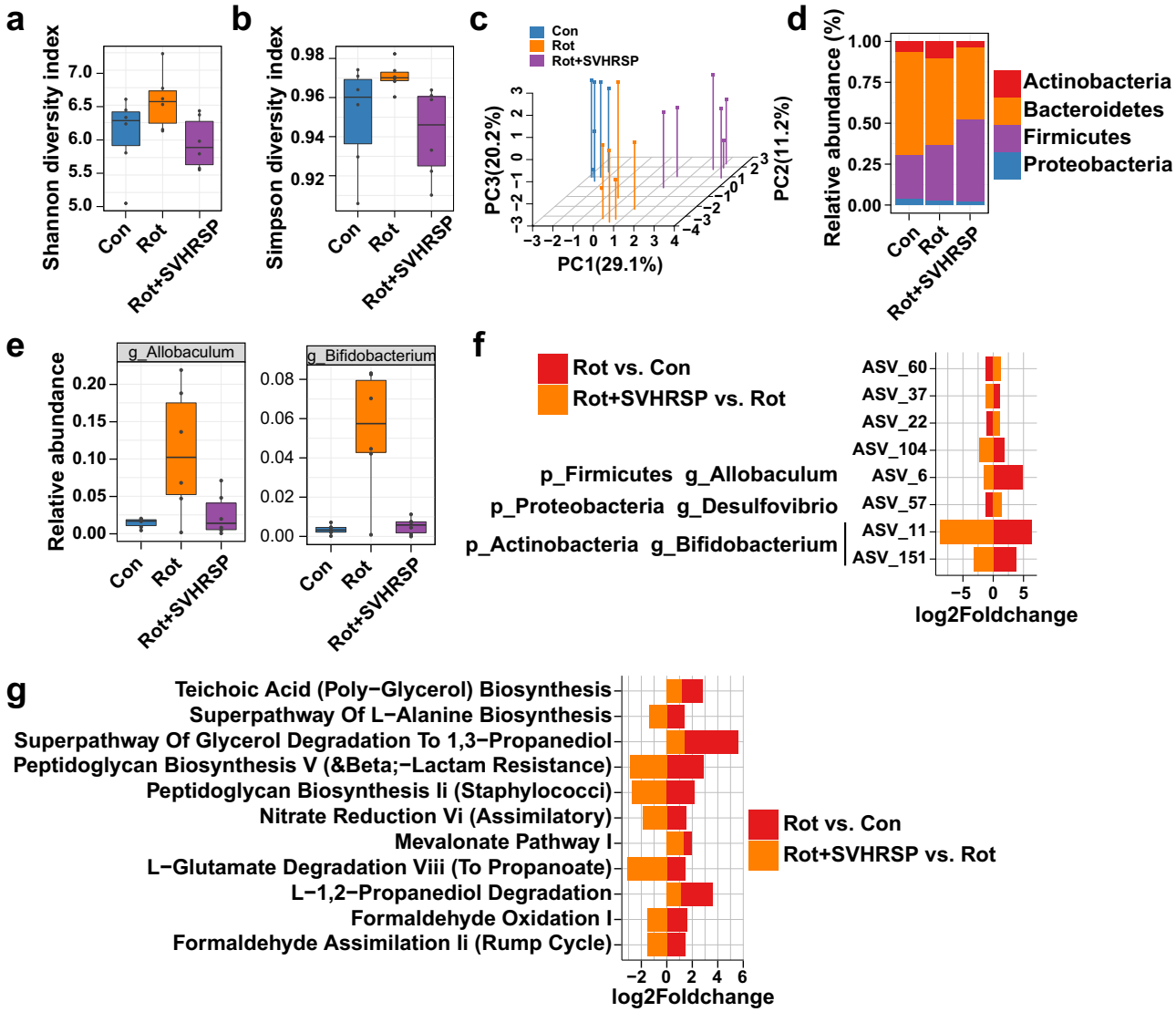

Fig. 2 | SVHRSP treatment mitigates dysbiosis in the fecal microbiota in rotenone-induced PD mice. a Alpha-diversity result of gut microbiota using Shannon index. **b** Alpha-diversity result of gut microbiota using Simpson index. **c** PCoA plots showing beta diversity via weighted UniFrac analysis across various groups. **d** Relative prevalence of gut microbiota at the phylum level. **e** Relative abundances of Bifidobacterium and Allobaculum in the three groups. **f** Bar plot showing the overlap of amplicon sequence variants (ASVs) between Rot versus Con and Rot + SVHRSP versus Rot, presented as log2fold change. ASVs are listed with corresponding genus or phylum levels. **g** Overlap of KEGG pathways in fecal pellets between Rot versus Con and Rot + SVHRSP versus Rot, depicted as log2fold change.

LC-MS (Fig.3 and Supplementary Fig. 1). PLS-DA clustering revealed distinct separation among three clusters, indicating significant differences in fecal metabolites among the Con, Rot, and Rot + SVHRSP group mice (Fig. 3a). We then identified the most highly differential metabolites in fecal pellets between the Rot group versus Con group and Rot + SVHRSP group versus Rot group comparisons. There were 54 metabolites identified between the Rot group and Con group mice, and 75 metabolites between the Rot + SVHRSP group and Rot group mice (Fig. 3b). A total of seven metabolites, including Epigallocatechin, (S)-Abscisic Acid, 3-epiecdysone, 3-methoxy-4-hydroxyphenylglycolaldehyde (MOPEGAL), Catechin, Cytosine, and 5,7-dihydroxyflavone, overlapped between the differential metabolites observed in the Rot group versus Con group and Rot + SVHRSP group versus Rot group comparisons (Fig. 3b, c). All seven metabolites were downregulated in the rotenone-induced PD mice compared with the Con group and were conversely upregulated in the Rot + SVHRSP group mice compared with the Rot group (Fig. 3c). Subsequently, we used MetaboAnalyst to conduct pathway enrichment analysis for the metabolites between the Rot + SVHRSP and Rot group mice (Fig. 3d). Further exploration of associations between the abundances of specific bacterial genera and differentially altered metabolites was performed. The abundances of some genera, such as Allobaculum and Bifidobacterium, showed significant correlations with the differentially altered metabolites (Fig. 3e).

Gut microbiota depletion mitigates the neuroprotective effects of SVHRSP in rotenone-induced PD mice

To investigate the role of gut microbiota in SVHRSP-mediated neuroprotection, mice were pretreated with antibiotics (Abx) for 3 weeks to deplete the microbiota, followed by rotenone and SVHRSP treatment (Fig. 4a). Consistent with previous findings[19], SVHRSP improved gait abnormalities and enhanced rotarod activities in rotenone-induced PD mice with gut microbiota (Fig. 4b, c). However, gut microbiota depletion using Abx significantly reduced the beneficial impact of SVHRSP on alleviating rotenone-induced gait abnormalities and decreased rotarod activity (Fig. 4b, c). We further investigated whether gut microbiota depletion affects SVHRSP-mediated neuroprotection in mice. SVHRSP treatment effectively attenuated the degeneration of dopaminergic neurons in both the SNpc and striatum in rotenone-treated mice with

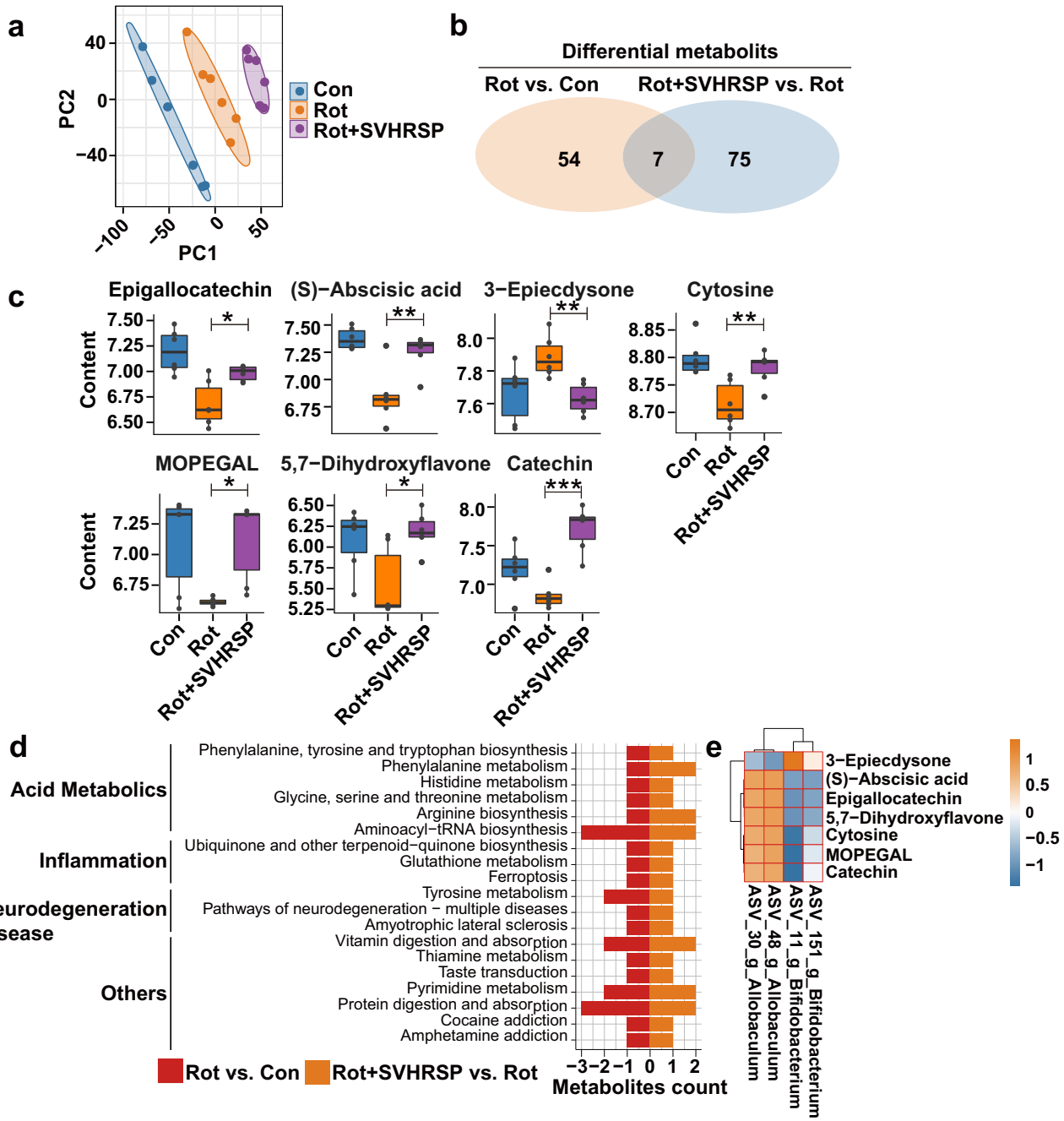

Fig. 3 | Fecal metabolism in rotenone PD mice and upon SVHRSP reversal. a PLS-DA plots of metabolites among different groups. **b** Examination of the number of differentially altered metabolites from Rot versus Con and from Rot + SVHRSP versus Rot. **c** Boxplot showing the levels of different metabolites across various groups. **d** Pathway overrepresentation analysis of differential metabolites for Rot + SVHRSP versus Rot. **e** Heatmap of the Spearman's correlation analysis between microbiota at the genus level and differentially altered metabolites among Con, Rot, and Rot + SVHRSP groups. $^{*}p < 0.05$, $^{**}p < 0.01$, $^{***}p < 0.001$.

gut microbiota (Fig. 4d). In contrast, the neuroprotective effects of SVHRSP against rotenone-induced dopaminergic neurodegeneration were significantly diminished by gut microbiota depletion (Fig. 4d). The role of gut microbiota in SVHRSP-mediated neuroprotection was further confirmed by assessing the expression of tyrosine hydroxylase (TH) and Neu-N protein in the SN of mice. SVHRSP treatment significantly prevented rotenone-induced reduction in TH expression in mice with gut microbiota, but not in mice with microbiota depletion (Fig. 4e). The results for Neu-N protein were similar to those for TH (Supplementary Fig. 2). Similarly, rotenone-induced Ser129-phosphorylation of α-synuclein was also significantly inhibited by SVHRSP in a microbiota-dependent way (Fig. 4e). Collectively these data indicate that gut microbiota depletion diminishes the neuroprotective effects of SVHRSP in rotenone-induced PD mice.

SVHRSP attenuates inflammation and intestinal barrier permeability in the colon of rotenone-induced PD mice

Given the distinct fecal metabolites between the rotenone-treated and rotenone and SVHRSP co-treated group mice, which were related to antioxidant and anti-inflammatory activities, we further examined the inflammatory changes within the intestinal tissue. HE staining of the colons revealed that SVHRSP exhibited protective effects against rotenone-induced immune cell infiltration in the mice's colons (Fig. 5a). Considering the pivotal role of the NF-κB pathway in gut inflammation,

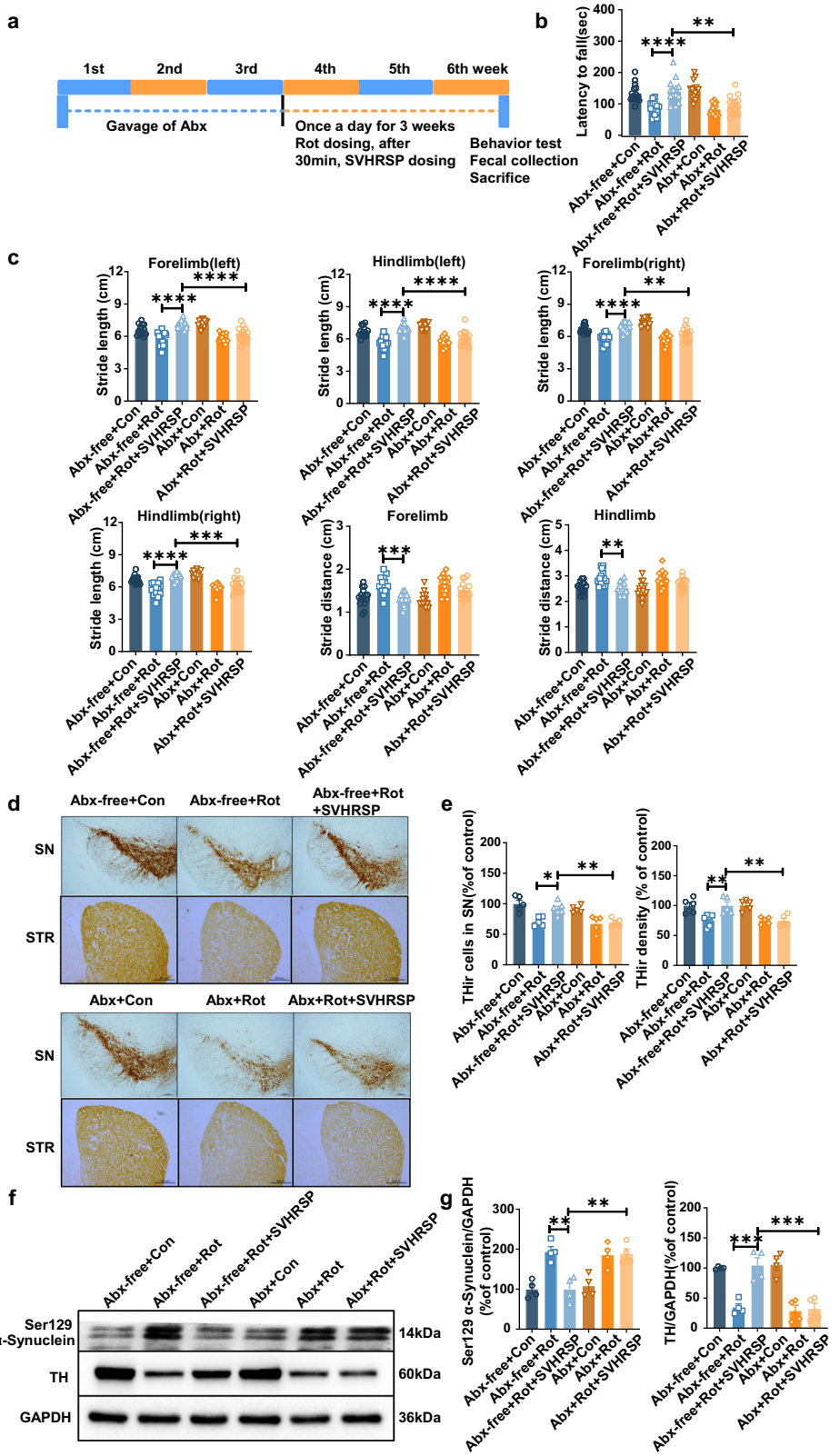

Fig. 4 | Gut microbiota depletion diminishes the neuroprotective effects of SVHRSP in rotenone-induced PD mice. a Experimental design: mice were administered mixed antibiotics once daily for 3 weeks, followed by rotenone and SVHRSP injection 30 min later. After 3 weeks, behavioral tests were conducted, and fecal samples were gathered from mice in each group. **b** Rotarod activities of mice with or without Abx. **c** Numerical outcomes of stride length and distance in both forelimb and hind limb of mice with or without Abx treatment ($n = 14–15$). **d** Representative images of TH immunostaining in the SN and striatum of mice. Scale bars represent 500 μm. **e** Measurement of the number of TH^+ neurons in the substantia nigra and the density of TH immunostaining in the striatum of mice ($n = 5–6$). **f** Representative bands of TH and Ser129-phosphorylated α-synuclein in the midbrain of mice. **g** Quantification of TH and Ser129-phosphorylated α-synuclein blots ($n = 4$). $^*p < 0.05$, $^{**}p < 0.01$, $^{***}p < 0.001$, $^{****}p < 0.0001$.

we assessed the impact of SVHRSP on its activation. Western blot analysis demonstrated an elevation in phosphorylated NF-κB in rotenone-treated mice, a response significantly mitigated by SVHRSP treatment, suggesting the inhibition of the NF-κB pathway (Fig. 5b). Additionally, SVHRSP treatment resulted in reduced mRNA levels of iNOS, TNF-α, and IL-1β in the colons of rotenone-treated mice (Fig. 5c). Overall, these results demonstrate that SVHRSP significantly mitigated immune infiltration and decreased the release of inflammatory factors in the colons of rotenone-treated mice.

Intestinal inflammation often triggers an increase in intestinal barrier permeability, resulting in the release of toxic factors into the periphery[15]. Therefore, we further examined the integrity of the

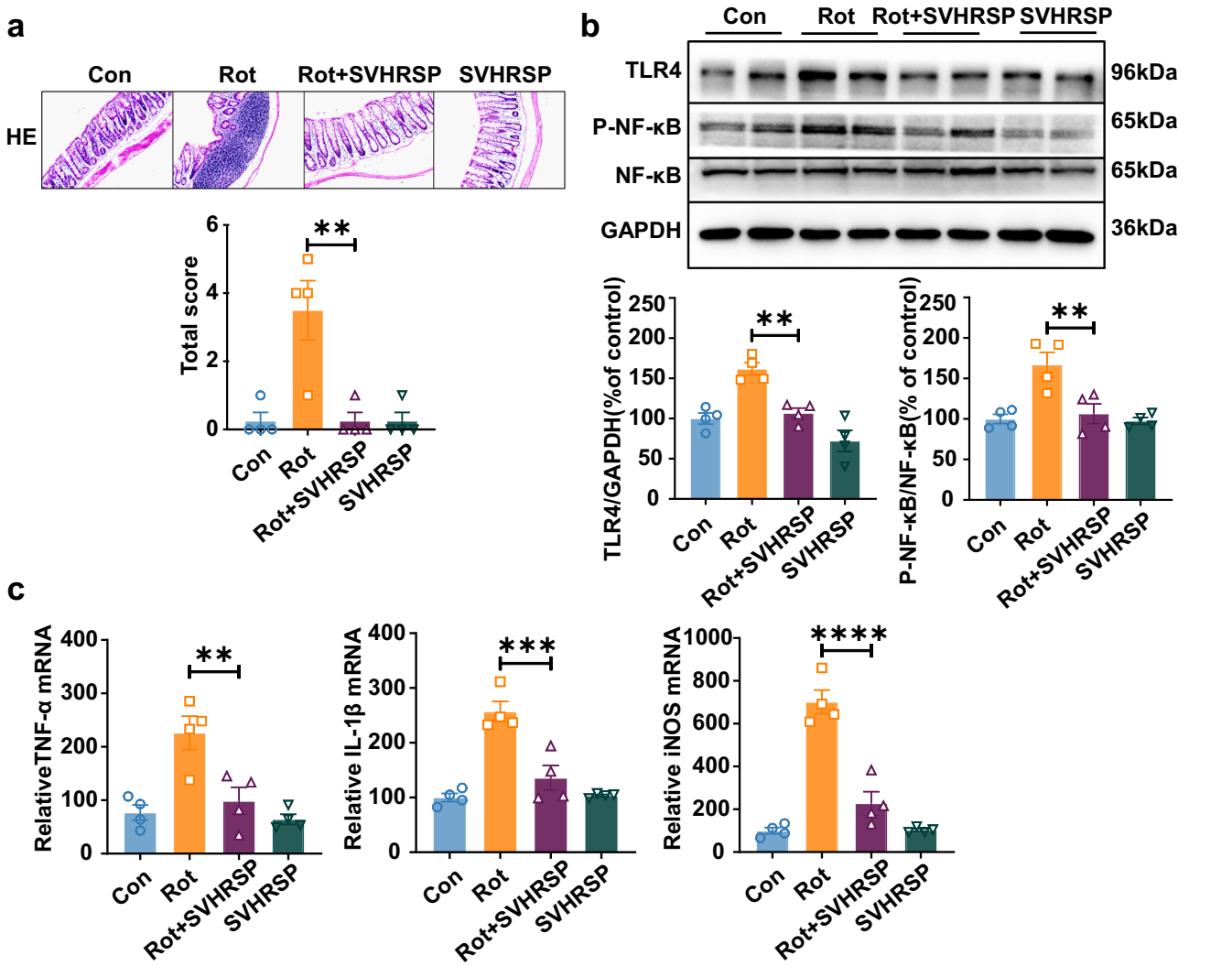

Fig. 5 | SVHRSP attenuates inflammation in the colon of mice among groups. **a** Representative images depicting H&E staining and corresponding histological scores in the colon of mice. Scale bars represent 200 μm. **b** Western blot bands of the expression levels of TLR4, phosphorylated, and total NF-kB in the colon of mice. **c** The mRNA expression levels of IL-1β, TNF-α, and iNOS in the colon of mice. $n = 4$. $^{**}p < 0.01$, $^{***}p < 0.001$, $^{****}p < 0.0001$.

intestinal barrier and the presence of inflammatory factors in the serum of mice. Western blot analysis indicated a notable decrease in the expression of the three major tight junction proteins, including Zonula occludens-1 (ZO-1), Claudin-1, and Occludin, in the colon of rotenone-treated mice compared to control mice. Remarkably, SVHRSP treatment markedly restored the expression of ZO-1, Claudin-1, and Occludin in rotenone-treated mice (Fig. 6a, b). Immunohistochemical staining of ZO-1 in the colon further supported the protective effect of SVHRSP against rotenone-induced decrease in tight junction protein (Fig. 6c, d).

To evaluate whether the restoration of intestinal barriers led to a decrease in the release of pro-inflammatory factors, we evaluated the content of lipopolysaccharide (LPS) and HMGB1, two common pro-inflammatory and toxic factors released due to gut dysbiosis, in the circulation. ELISA analysis showed a notable increase in the extent of both LPS and HMGB1 in the serum of rotenone-treated mice, which were notably decreased by SVHRSP treatment (Fig. 6e).

SVHRSP elevates BBB integrity via gut microbiota in rotenone-induced PD mice

The entry of pro-inflammatory molecules from the intestine into the systemic circulation may result in disruption of BBB, enabling inflammatory cytokines to enter the brain and trigger an inflammatory response. Neuroinflammation is a key factor in the ongoing neurodegenerative process seen in PD. To further survey the role of gut microbiota in SVHRSP-mediated neuroprotection in PD, we evaluated changes in BBB permeability and neuroinflammation in the presence or absence of gut microbiota. Western blot analysis showed a significant decrease in fibrinogen, a marker for BBB permeability, in mice co-treated with rotenone and SVHRSP compared to mice treated with rotenone alone. Conversely, Abx-mediated microbiota depletion nullified the reduction effects of SVHRSP against rotenone-induced fibrinogen accumulation in the brains of mice, indicating that the protective effects of SVHRSP against rotenone-induced increases in BBB permeability in mice are mediated by the gut microbiota (Fig. 7a). This finding was further reinforced by the detection of the expression of ZO-1, Claudin-5, and Occludin, three major tight junction proteins for the BBB. SVHRSP restored the expression of these tight junction proteins in rotenone-treated mice with microbiota, but not in mice without microbiota (Fig. 7b, c).

SVHRSP inhibits microglial activation and the activation LPS/HMGB1/TLR4/NF-κB pathway via gut microbiota in rotenone-induced PD mice

Due to the increased levels of LPS and HMGB1 in the serum of rotenone-treated mice, we hypothesized that pathogenic LPS and HMGB1 might enter the brain through a disrupted BBB, leading to

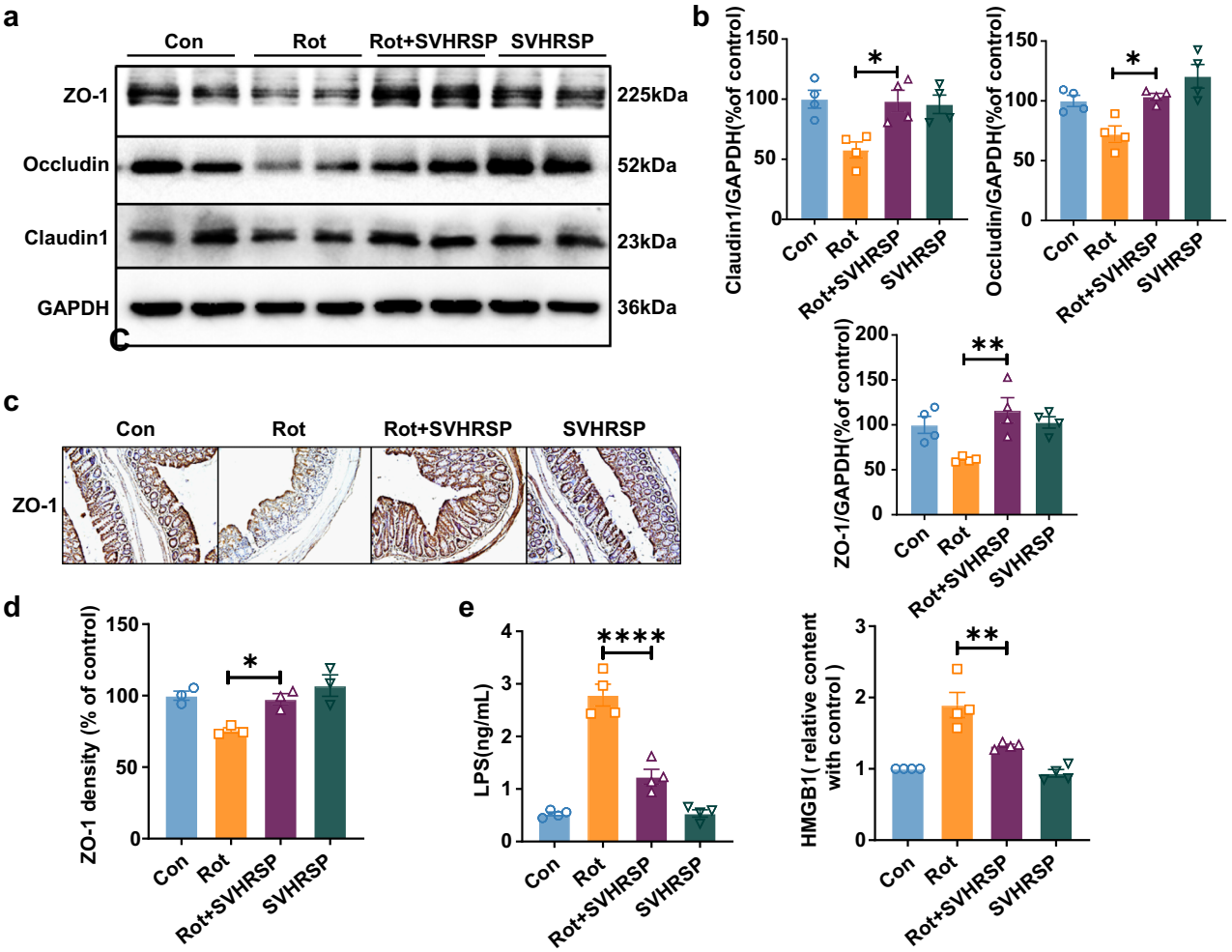

Fig. 6 | SVHRSP decreases intestinal barrier permeability in the colon and reduces the contents of LPS and HMGB1 in the serum of rotenone-induced PD mice. a Representative western blot bands of ZO-1, Claudin-1, and Occludin in the colon. **b** Quantitative assessment of ZO-1, Claudin-1, and Occludin expression. **c** Representative images of ZO-1 immunostaining in the colon. Scale bars represent 250 μm. **d** Statistical result of ZO-1 density. **e** Levels of LPS and HMGB1 in mouse serum. $n = 4$. $^{*}p < 0.05$, $^{**}p < 0.01$, $^{****}p < 0.0001$.

microglia-mediated neuroinflammation. Increased LPS and HMGB1 were observed in the brains of rotenone-treated mice, and this was significantly reduced by SVHRSP. Interestingly, microbiota depletion notably diminished the inhibitory effects of SVHRSP against rotenone-induced increases in LPS and HMGB1 in mice (Fig. 8a, b). Furthermore, SVHRSP treatment also microbiota-dependently inhibited rotenone-induced activation of microglia in the brain, as evidenced by decreased density of Iba-1 immunostaining in mice co-treated with rotenone and SVHRSP compared with mice treated with rotenone alone (Fig. 8c, d). Western blot analysis showed a reduction in the expression of CD11b, another marker for microglial activation, in SVHRSP-treated mice with the presence of microbiota (Fig. 8e, f). A previous study demonstrated that both LPS and HMGB1 can induce microglial activation through the TLR4-dependent pathway[21]. The effects of SVHRSP on rotenone-induced expression and activation of the TLR4 and NF-κB signaling pathway were determined. In line with the inhibition of microglial activation, SVHRSP reduced rotenone-induced TLR4 expression and NF-κB activation in the brains of mice with microbiota, but not in those with Abx-mediated microbiota depletion (Fig. 8e, f). Additionally, the mRNA levels of TNF-α and iNOS in the brain of mice showed the similar results (Fig. 8g, h). In summary, these findings underscore the role of gut microbiota in the SVHRSP-induced inhibition of neuroinflammation in the rotenone mouse PD model.

FMT from SVHRSP mice attenuates dopaminergic neurodegeneration and motor deficits in rotenone-induced PD mice

The above results suggest that SVHRSP exerts neuroprotective effects in a rotenone-induced mouse PD model by reshaping the gut microbiota. To further confirm gut microbiota remodeling mediates the neuroprotective effects of SVHRSP, we obtained fecal samples from mice treated with both rotenone and SVHRSP. These samples were transplanted into mice treated with rotenone alone for 21 days, forming the Rot + FMT (fecal microbiota transplantation) group (Fig. 9a). Mice in the Rot + FMT group showed improved gait performance and rotarod activities compared to those in the Rot alone group (Fig. 9b, c). Immunostaining for TH^{+} neurons and western blot analysis of TH expression further confirmed that FMT attenuated rotenone-induced degeneration of dopaminergic neurons in the nigrostriatal pathway in mice (Fig. 9d–g). Additionally, electron microscopy revealed that the mitochondria in rotenone-treated mice were swollen with reduced mitochondrial cristae and indistinct axonal synapses, which were also notably attenuated by FMT (Fig. 9h). These findings further validate the important role of gut microbiota in mediating the protective efficacy of SVHRSP.

Discussion

In this study, we explored how the gut microbiota influences the neuroprotective benefits of SVHRSP in a mouse model of PD induced by rotenone. Our results showed that SVHRSP improved gastrointestinal

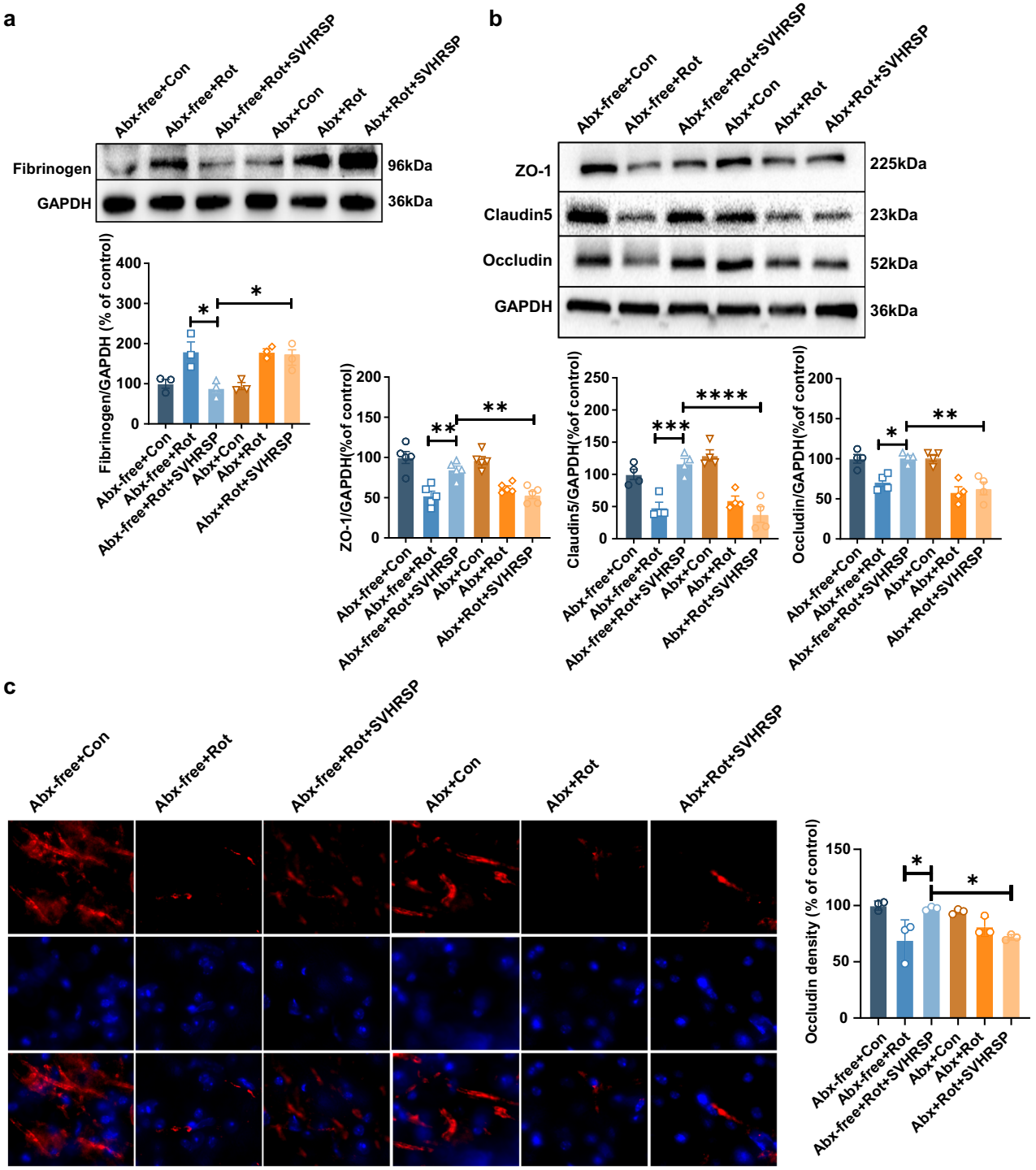

Fig. 7 | SVHRSP elevates BBB integrity via gut microbiota in rotenone-induced PD mice. a The representative image and quantitative analysis of fibrinogen blot in the midbrain of mice. $n = 3$. **b** The representative images and quantitative analysis of Occuldin, Claudin-5, and ZO-1 in the midbrain of mice. $n = 4–5$. **c** The representative images and quantitative analysis of Occludin immunostaining in the midbrain of mice. Scale bars represent 20 μm. $n = 3$. $^{*}p < 0.05$, $^{**}p < 0.01$; $^{***}p < 0.001$, $^{****}p < 0.0001$.

function, modified the composition and metabolites of gut microbiota, and reduced intestinal barrier damage and the release of toxic factors into the bloodstream in rotenone-treated mice. Consumption of gut microbiota reduced the neuroprotective effects, while FMT from SVHRSP co-treated mice replicated the dopaminergic neuroprotection seen in rotenone-induced PD mice. Additionally, we observed that SVHRSP inhibited rotenone-induced microglial activation in the SN and the activation of the TLR4/NF-κB pathway in a microbiota-dependent manner. These findings suggest that SVHRSP's ability to protect neurons might involve reshaping the composition of gut bacteria to perform anti-inflammatory roles.

PD patients and animal models exhibited notable variances in both the abundance and composition of gut bacteria compared with controls[22,23]. 16S rRNA gene sequencing of fecal samples demonstrated that SVHRSP treatment resulted in alterations of gut microbiota abundance and diversity compared to the PD mouse model, with a notable increase in species like

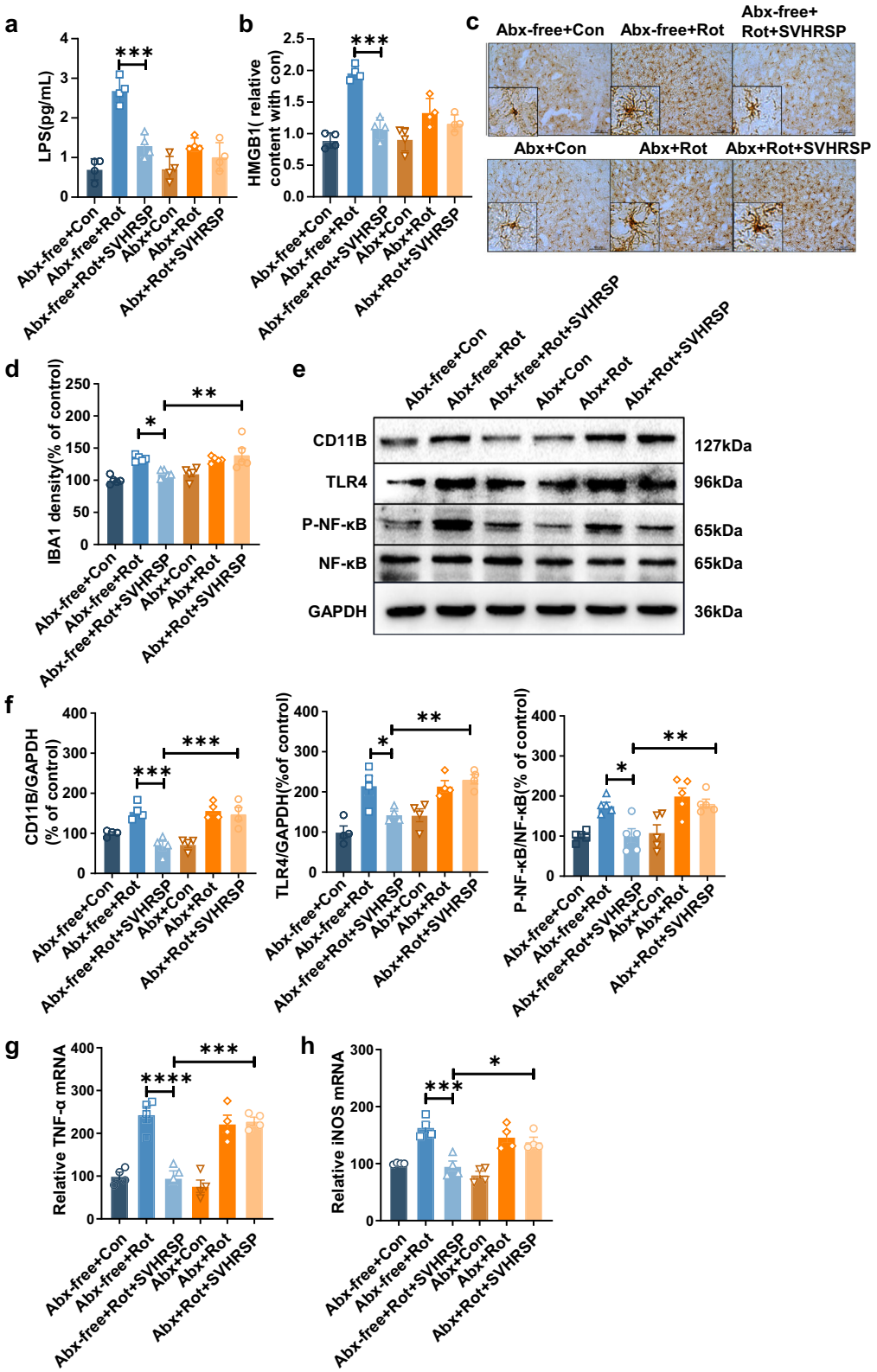

Fig. 8 | SVHRSP inhibits microglial activation and TLR4/NF-κB pathway activation via gut microbiota in rotenone-induced PD mice. Levels of LPS (**a**) and HGM1 (**b**) in serum measured by ELISA ($n = 4$). Representative images (**c**) and statistical analysis (**d**) of Iba-1 immunostaining in the substantia nigra (SN) of mice ($n = 5$). Scale bars represent 100 μm. Representative western blots (**e**) and densitometry analysis (**f**) of CD11b, TLR4, NF-κB, and P-NF-κB in the midbrain tissues of mice ($n = 4$). The mRNA expression levels of TNF-α (**g**) and iNOS (**h**) in the midbrain of mice ($n = 4$). *$p < 0.05$, **$p < 0.01$, ***$p < 0.001$, ****$p < 0.0001$.

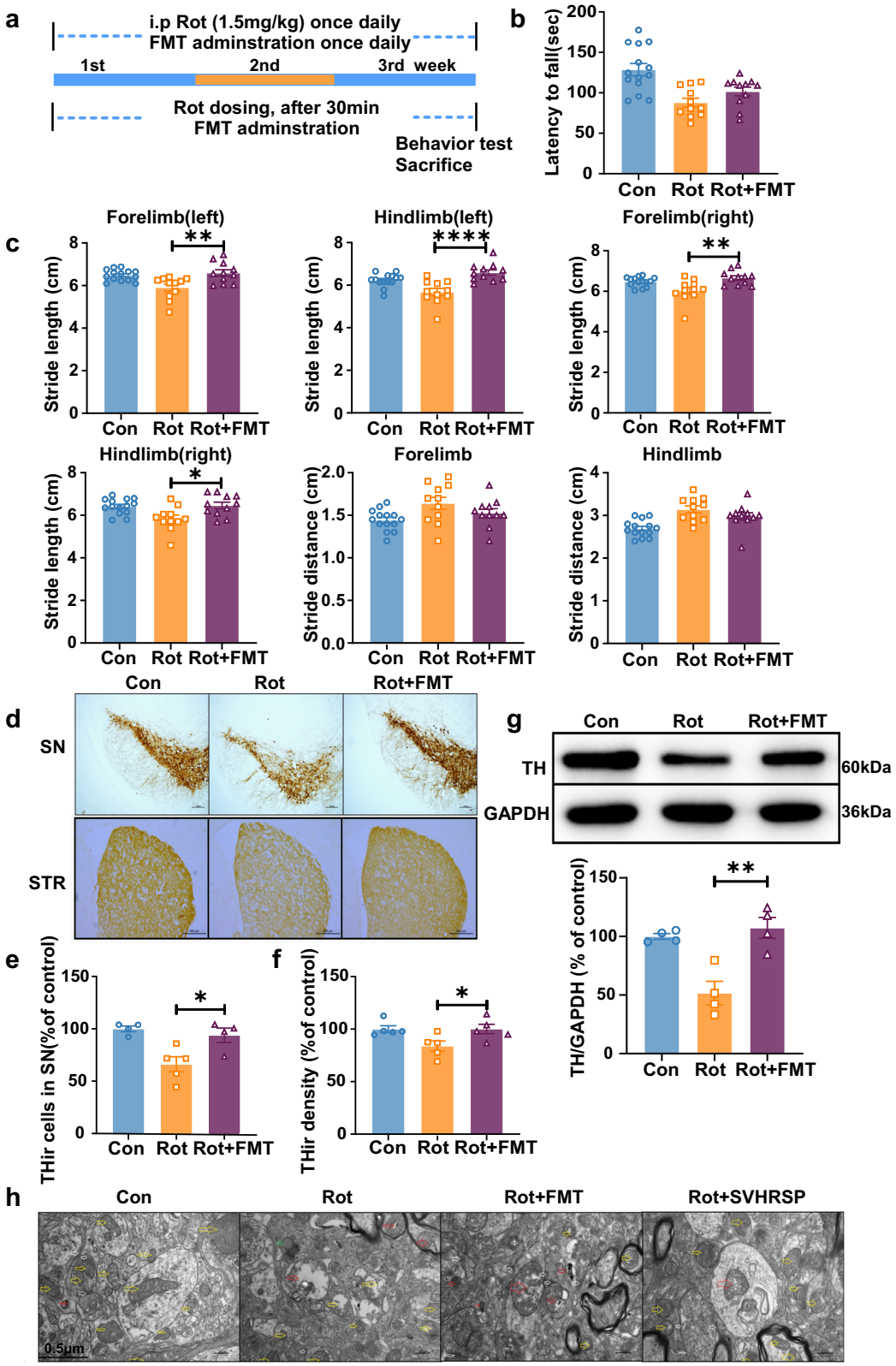

Fig. 9 | FMT from SVHRSP mice mitigates dopaminergic neurodegeneration and motor impairments in rotenone-induced PD mice. a Experimental design: mice in the Rot group received daily rotenone treatment for 3 weeks, whereas mice in the Rot + FMT group were first administered rotenone, followed by fecal microbiota freshly prepared from Rot + SVHRSP mice. Behavioral tests were conducted following 3 weeks of rotenone treatment. **b** Rotarod activity. **c** Gait performance. $n = 11–14$. **d** Immunostaining of TH+ neurons in the substantia nigra (SN) and striatum of mice. Scale bars represent 500 μm. **e** Quantitative assessment of the number of TH+ neurons in the substantia nigra pars compacta (SNpc). **f** Density of TH immunostaining in the striatum. **g** The protein expression levels of TH in the midbrain of mice were evaluated using western blot. **h** Electron microscopy showing the morphology of mitochondria in the SN. $n = 4–5$. $^{*}p < 0.05$, $^{**}p < 0.01$, $^{****}p < 0.0001$.

Allobaculum. While alterations in other bacterial strains were observed between SVHRSP co-treatment mice and rotenone alone mice, the most significant changes were observed in Allobaculum strains. A previous study reported an increase in Allobaculum species in a PD rat model[24], which can degrade mucin, leading to increased intestinal permeability and inflammation. This phenomenon is analogous to what is observed in diabetic mice that are fed a high-fat diet[25,26]. The function of gut microbiota in SVHRSP-mediated protection was further investigated by depleting gut microbiota. Gut microbiota depletion, typically achieved via Abx treatment, is a commonly employed approach to explore the role of microbiota in the neuropathology of neurodegenerative disease models[17]. Our research showed that a reduction in gut microbiota using Abx attenuated the neuroprotective effects of SVHRSP on behavioral abnormalities, dopaminergic neuron loss, and the expression of TH and α-synuclein proteins. Additionally, FMT from mice co-treated with Rot and SVHRSP also ameliorated rotenone-induced behavioral abnormalities, dopaminergic neuron loss, and mitochondrial morphological abnormalities in mice. These findings underscore the therapeutic potential of fecal microbiota derived from mice co-treated with SVHRSP in the PD mouse model. In alignment with our findings, the pivotal role of gut microbiota in other potential anti-PD drugs has also been reported. Cui et al. discovered that curcumin treatment effectively alleviated motor deficits and neuropathological changes in a mouse model of PD induced by MPTP, which were linked to an improved balance of gut flora. Microbiota depletion mediated by ABX confirmed that the gut microbiota was necessary for the protective effects of curcumin in MPTP-induced PD mice[17]. Similarly, through ABX and FMT experiments, Hou et al. demonstrated the role of gut microbiota in the neuroprotective effects of osteocalcin, an osteoblast-secreted protein, in a mouse model of PD induced by 6-hydroxydopamine (6-OHDA)[8].

We then investigated the mechanisms through which SVHRSP exerts neuroprotective effects by modulating the gut microbiota. Our metabolomics profiling of mouse fecal samples revealed differences in metabolites primarily associated with oxidative stress and inflammatory responses between the SVHRSP and rotenone co-treated groups and the rotenone alone group. The differential metabolites included epigallocatechin, (S)-abscisic acid, 3-epiecdysone, 3-methoxy-4-hydroxyphenylglycolaldehyde, catechin, cytosine, and 5,7-dihydroxyflavone. Importantly, most of the identified metabolites have been reported to reduce neuronal damage in PD models, in both in vivo and in vitro studies. For instance, (S)-abscisic acid has been shown to alleviate neuronal damage induced by 6-OHDA[27] and inhibit protein expression related to neuroinflammation in an in vitro PD model[28]. Catechin is also effective in preventing neuronal damage in a 6-OHDA cell PD model[29], while 5,7-dihydroxyflavone has shown anti-oxidative properties on dopaminergic neurons in PD[30]. MOPEGAL is a metabolite derived from the breakdown of neurotransmitters like norepinephrine and epinephrine[31]. Norepinephrine has been reported to provide potent dopaminergic neuroprotection in both in vivo and in vitro PD models[32]. These differential metabolites not only further demonstrate the neuroprotective effect of SVHRSP but also suggest that anti-inflammatory and antioxidant mechanisms contribute to SVHRSP-afforded neuroprotection.

Multiple studies have shown that in various PD mouse models, the intestinal barrier is compromised, leading to elevated levels of intestinal inflammation and increased serum levels of inflammatory factors, as well as upregulation of inflammation-related proteins in the midbrain region[33]. Intestinal inflammation, in turn, can increase intestinal barrier permeability, potentially allowing inflammatory and toxic factors to enter the bloodstream[16]. The increased permeability of the intestinal barrier and the presence of toxic factors, such as LPS and HMGB1, in the serum were detected in rotenone-induced PD mice. Notably, SVHRSP significantly blocked the rotenone-induced increase in intestinal barrier permeability and the release of LPS and HMGB1. Similarly, other neuroprotective drugs, such as Eucommiae and Sodium Butyrate, can also mitigate the disruption of the intestinal barrier and inhibit inflammation[34,35]. Inflammatory and toxic factors in the blood can target the BBB, increasing its permeability and allowing toxic factors to enter the brain, triggering inflammation and neuronal damage[26]. We hypothesize that the inhibitory effects of SVHRSP on intestinal and peripheral inflammation could alleviate BBB damage and the subsequent entry of toxic factors into the brain, thereby reducing neuroinflammation. The findings from this study indicated elevated levels of fibrinogen and reduced expression of tight junction proteins in the brains of PD mice induced by rotenone, which were significantly attenuated by SVHRSP in a microbiota-dependent manner. Additionally, SVHRSP and rotenone co-treated mice showed reduced levels of LPS and HMGB1, as well as decreased microglial activation and expression of the TLR4/NF-κB pathway compared to mice treated with rotenone alone. Importantly, these protective effects of SVHRSP were found to be dependent on gut microbiota. These results suggest that SVHRSP reduced BBB permeability, brain entry of toxic factors, and neuroinflammation by inhibiting intestinal inflammation through reshaping the gut microbiota. Similarly, using an MPTP-induced mouse PD model, Dong et al. discovered that a polysaccharide derived from brown seaweed, specifically polymannuronic acid, notably enhanced the integrity of both the intestinal barrier and the BBB. This compound also mitigated inflammation in the gut, brain, and systemic circulation by modulating the brain-gut-microbiota axis. PM treatment significantly reduced the mRNA expressions of pro-inflammatory cytokines in the mice colon, and improved ZO-1 and occludin mRNA expressions in either the colon or SNpc of PD mice[36].

Although the protective effect of SVHRSP on the intestine has been confirmed in this study, it remains unclear whether this protection is dose-dependent. Furthermore, the potential correlation between the time course of SVHRSP-induced improvement of colon disorder and the protection of dopaminergic neurons has not been investigated. Therefore, these may be the focus of our future research.

Methods

Reagents

Rotenone (Rot, R8875) was obtained from Sigma-Aldrich (St. Louis, MO, USA). LPS (437627) was purchased from Merck Millipore (Darmstadt, Germany). The antibodies against tyrosine hydroxylase (TH, 25859-1-AP), Zonula occludens-1 (ZO-1, 21773-1-AP), Occludin (27260-1-AP), Claudin-1 (13050-1-AP), Toll-like receptor 4 (TLR4, 66350-1-Ig), and HMGB1 (10829-1-AP, Proteintech, Wuhan, China) were purchased from Proteintech (Wuhan, China). The anti-ionized calcium-binding adapter molecule-1 (Iba-1, 019-19741) was purchased from Wako Chemicals (Tokyo, Japan). The antibodies against Claudin-5 (VB298617) and Alexa FluorTM594 goat anti-rabbit IgG (A11012) were purchased from Invitrogen (Waltham, USA). The antibodies against ser129-α-synuclein (ab51253) and CD11b (ab133357) were purchased from Abcam (Cambridge, UK). The antibodies against GAPDH (ABL1020) and anti-rabbit IgG (A21020) were purchased from Abbkine (Wuhan, China). The anti-mouse IgG (7076S) was purchased from Cell Signaling Technology (Boston, USA). The ELISA kit LPS (CSB-E13066m) was purchased from CUSABIO Biology (Wuhan, China).

Animal treatment

Adult male C57BL/6 mice were maintained in a standard laboratory provided with access to both food and water, and then partitioned into four distinct groups ($n = 15$/group): control (Con), rotenone (Rot), rotenone + SVHRSP (Rot + SVHRSP), and SVHRSP alone. Rotenone was prepared daily using 0.1% DMSO and 10% PEG400 in normal saline, following previous reports with minor modifications[37–39]. Mice in the Rot group were administered intraperitoneal injections of 1.5 mg/kg/day rotenone for 3 consecutive weeks. Mice in the Rot + SVHRSP groups were treated with SVHRSP (0.4 mg/kg) 30 min after each rotenone injection. The control group mice received an equivalent volume of vehicle. All animal care and experimental procedures were conducted in accordance with the principles

and guidelines outlined in the National Institutes of Health Guide for the Care and Use of Laboratory Animals under the approval of animal ethics document number AEE22008.

Antibiotics treatment

Adult male C57BL/6 mice were allocated to either the antibiotic (Abx)-free group or the Abx group ($n = 45$/group) through a randomized process. Each of these two groups was further subdivided into three groups: Con, Rot, and Rot + SVHRSP ($n = 15$/group). The antibiotic solution, consisting of Ampicillin 200 mg/kg, Neomycin 200 mg/kg, Vancomycin hydrochloride 100 mg/kg, and Metronidazole 200 mg/kg in saline, was freshly prepared as previously described[40–42]. The mice were given the combination of antibiotics once daily for three consecutive days. Subsequently, the treatment of rotenone and SVHRSP in both the Abx-free and Abx group mice was consistent with the aforementioned protocol.

Fecal microbiota transplantation

In the FMT experiment, mice were randomly allocated into Con, Rot, and Rot + FMT groups ($n = 15$/group). Mice in the Rot group were administered 1.5 mg/kg/day rotenone (i.p.) for 3 consecutive weeks. Mice in the Rot + FMT groups received FMT (100 μL) by gavage 30 min after each rotenone injection. The fecal microbiota was prepared from mice according to a previous protocol[43]. Briefly, fresh fecal samples from mice in the Rot + SVHRSP group were collected and immersed in sterile saline solution (100 mg feces/1 mL physiological saline) for 1 min. The fecal solution was homogenized, followed by centrifugation at 1000 × *g*, 4 °C for 3 min. Then, the supernatant (100 μL) was administered to mice in the Rot + FMT group within 10 min. The control group mice received an equivalent volume of vehicle.

Gait measurement

Gait analysis was used to evaluate the motor behavior of mice according to previous studies[19,44]. The mice were led along a darkened box measuring 50 cm in length and 10 cm in width. Different colored dyes were applied to the fore and hind limbs of the mice, leaving footprints on paper. Two distinct footprints were chosen for each mouse, and the distances between the left forelimb, left hind limb, right forelimb, and right hind limb were measured, as well as the interlimb distances for both forelimbs and hind limbs.

Rotarod

The rotarod experiment was employed to assess the movement coordination of mice by measuring the length of time they were able to maintain their balance on the rotating rod. Before the actual test, the mice underwent 3-day training on the rotarod, at a speed of 4 revolutions per minute (r.p.m) for 5 min each day. In the formal assessment phase, mice were positioned on the accelerating rod, which ranged from 4 to 40 r.p.m, and the duration of their retention was documented. Each mouse underwent three times and the mean duration was computed for subsequent analysis[45].

One-hour stool collection

On the final day of the experiment, the mice were subjected to a 12-h fasting period. Following this, each mouse was individually housed in a sanitized cage for a 1-h observation session. Feces were promptly collected after expulsion and transferred to sterilized tubes. The frequency of defecation and fecal weight were recorded. In line with previous studies[46], fecal moisture content (%) was determined using the following formula: (wet weight − dry weight)/wet weight × 100%.

Intestinal transit distance and colon length measurement

The mice underwent a 12-h fasting period before the experiment. The following day, they were administered ink and euthanized 30 min later. The subsequent step involved measuring the length from the pylorus to the furthest position of the ink in the colon[47,48].

16S rRNA sequencing and metabolomics

According to a previously published method for detecting 16S rRNA[47], mice were selected at random from each group for microbiota sequencing analysis. Each mouse was individually placed in an individual empty sterilized cage, and 3–4 fresh fecal pellets were obtained from each mouse. The gathered fecal pellets were immediately transferred into a sterile EP tube. The fecal samples were preserved at −80 °C for subsequent processing. The fecal samples were sent to PANOMIX Company for library construction and sequencing. Microbial genomic DNA was acquired using the QIAamp Fast DNA Stool Mini Kit (Qiagen, Germany), and the V3–V4 regions of the 16S RNA gene were amplified with the paired primers (forward primer: 5′-CCTACGGGRS GCAGCAG-3′; reverse primer: 5′-GGACTACVVGGG TATCTAATC-3′). Sequencing libraries were constructed using the TruSeq DNA LT Sample Preparation Kit (Illumina, Catalog No. FC-121-2001). DNA sequencing was conducted using an Illumina HiSeq 2500 platform to generate paired-end reads with a length of 250 base pairs.

Fecal samples from different groups were collected and sent to PANOMIX Company for metabolite detection. The fecal metabolites were then extracted using MeOH, which contained 2-Amino-3-(2-chloro-phenyl)-propionic acid (4 ppm)[49], and detected using a Vanquish UHPLC System and Q Exactive (Thermo Fisher Scientific, USA) with an ESI ion source[50,51].

Bioinformatic analysis

We primarily analyzed sequence data using QIIME2 and R software (v3.6.0). Alpha-diversity indices at the ASV level were computed using the AS table in QIIME2. Beta diversity analysis was carried out to examine the heterogeneity in microbial community structure across samples using UniFrac distance metrics. The distinction of microbiota composition among groups was evaluated using ANOSIM (Analysis of similarities) in QI2. R was utilized to visualize the taxonomic profiles and relative abundance.

The initial step involved converting the raw metabolic data into mzXML format using MSConvert in the ProteoWizard software package (v3.0.8789) and processed with R XCMS (v3.12.0) for feature detection, retention time correction, and alignment. Subsequently, batch effects were removed, and high-quality metabolites were filtered for further data analysis. Metabolites were recognized using accurate mass and the MS/MS database. PLS-DA was performed using the R ropls (v1.22.0) package. The enriched pathways of differential metabolites were analyzed using MetaboAnalyst. The metabolites along with their associated pathways were graphically using the R ggplot2 package.

Hematoxylin and eosin (HE) staining

The mice were flushed with PBS, followed by 4% paraformaldehyde (PFA). Then, the colon located below the cecum was collected and was immersed in 4% formalin for 48 h. Then, the tissue was paraffin-embedded, cut into sections, and stained with HE. Subsequently, the pathological alterations in the colon tissue were evaluated and randomly scored as shown in Table 1.

Table 1 | The criteria for histological analysis of the colonic damage score

Score	0	1	2	3	4
Crypt damage	None	Basal 1/3	Basal 2/3	Crypt loss	Crypt and surface epithelial destruction
Inflammation severity	None	Mild	Moderate	Severe	
Inflammation infiltration	None	Mucosa	Mucosa and submucosa	Transmural	

Table 2 | Primers list

Reagent	Forward	Reverse
GAPDH	5′-TTCAACGGCACAGTCAAGGC-3′	5′-GACTCCACGACATACTCAGCACC-3′
ZO-1	5′-CATCTCCAGTCCCTTACCTTTC-3′	5′-CCTCCAGGCTGACATTAGTTAC-3′
Occludin	5′-GAGCTTACAGGCAGAACTAGAC-3′	5′-CAGCCATGTACTCTTCACTCTC-3′
Claudin-1	5′-GGTTATCGGAACTGTGGTAGAA-3′	5′-GTGCTCAGGGAAGATGGTAAG-3′
TNFα	5′-GACCCTCACACTCAGATCATCTTCT-3′	5′- CCTCCACTTGGTGGTTTGCT-3′
IL-1β	5′-TGACCTGTTCTTTGAGGCTGAC-3′	5′-GATGCTGCTGTGAGATTTGAAG-3′
iNOS	5′-CTGCCCCCCTGCTCACTC-3′	5′-TGGGAGGGGTCGTAATGTCC-3′

Immunohistochemistry

For immunohistochemistry, mice were initially flushed with PBS, followed by 4% PFA. The brains were cut and then immersed in 4% PFA at 4 °C for 48 h, followed by immersion in a 30% sucrose solution for 2 days. Subsequently, the brains were sectioned into 30 μm slices using a Leica CM1950 cryostat (Leica Biosystems, Germany) based on previous research[52]. Slices containing the SN region spanning approximately −2.46 mm to −4.0 mm[53,54] or the striatum from approximately 1.10–0.02 mm relative to Bregma coordinates (Paxinos and Watson, 2006) were collected. After sectioning, brain slices underwent a series of procedures: a triple wash with PBS, a 15-min incubation with 3% H_2O_2 to deactivate endogenous peroxidase activity, followed by a 1-h blocking step in a solution comprising 4% goat serum, 0.3% TritonX-100, and 1% BSA dissolved in PBS. Subsequently, brain slices were incubated overnight at 4 °C with TH (1:1000), Iba-1 (1:500), and ZO-1 (1:250) antibodies. The following day, the sections were treated with anti-rabbit IgG for 2 h, followed by processing using an avidin–biotin complex (ABC) kit and visualization using 3,3′-diaminobenzidine. Digital slide scanners were used for image capture.

The quantification of TH-positive neurons was carried out following established procedures[55]. Every three sections from the rostral of a series of 24 sections that cover the entire extent of SN were selected for immunostaining[56]. The total number of THir neurons in the SNpc was counted manually by two individuals blind to the treatment. The final count was obtained by averaging their counting results. Previous reports demonstrated that it's rather consistency for quantification of THir neurons in mice between manual and stereology counts[57,58].

Density analysis of Iba-1 or ZO-1 was performed utilizing ImageJ software. Staining images underwent conversion into 32-bit grayscale image, followed by the selection and measurement of both background and quantified areas. Data were relatively quantified by analyzing pixel density within specific brain regions, calculated as total pixels per area[2,44].

Western blot

Equal amounts of brain tissue samples from each mouse were weighed and homogenized in ice-cold RIPA buffer with added PMSF (at a ratio of 1:100) and protease and phosphatase inhibitors (at a ratio of 1:200). The homogenates were then shaken, thoroughly mixed, and centrifuged at 10,000 × *g* for 15 min. The resulting supernatant was gathered, and the protein concentration was assessed using the BCA Assay. Subsequently, the proteins were adjusted to a consistent concentration, mixed with 5× loading buffer, and boiled at 100 °C for 5 min. Equal amounts of proteins were loaded on an 8%–12% Bis–Tris-polyacrylamide gel and subsequently transferred onto poly-vinylidene fluoride membranes. These membranes were blocked at room temperature for 2 h using Tris-buffered saline and Tween-20 (TBST) with 5% nonfat milk. Subsequently, they were left to incubate overnight at 4 °C with antibodies against TH (1:1000), α-synuclein (1:500), TLR4 (1:800), NF-kB (1:1000), P-NF-kB (1:1000), Fibrinogen (1:1000), ZO-1 (1:1000), Occludin (1:1000), Claudin-5 (1:1000), CD11b (1:1000), and GAPDH (1:5000). The following day, the membranes were washed three times with TBST and then incubated at room temperature for 2 h with anti-rabbit IgG (1:5000) and anti-mouse IgG antibodies (1:5000). After incubation, the membranes were washed three times, and the bands were detected using ECL reagents. All blots or gels were derived from the same experiment and they were processed in parallel.

qRT-PCR

The tissue's RNA was extracted using TRIzol reagent (Invitrogen, Carlsbad, CA, USA). Subsequently, the purity and integrity of RNA were measured using the NanoDrop2000 instrument. Only samples with RNA purity between 1.8 and 2.0 were included in subsequent experiments. Following that, the RNA was reverse transcribed into cDNA employing the Evo MuLV RT kit (Accurate Biology®, China). Real-time PCR analysis was carried out on an Agilent Mx3005P instrument employing the SYBR Green Pro Taq HS qPCR kit[59]. The primer sequences are listed in Table 2.

ELISA assay

For HMGB1 assay, the 96-well plate was coated manually with HMGB1 antibody (1 μg/mL; 100 μL/well) overnight at 4 °C. Subsequently, the plate was flushed once with wash buffer and then blocked with 1% BSA for 1 h at room temperature. Serum or midbrain tissue samples of mice (100 μL/well) were introduced into the wells that had been coated with antibody HMGB1 and were incubated for 2 h at RT. After 1 h of incubation, the wells were washed with washing buffer and then were incubated with HRP-conjugated goat anti-rabbit IgG secondary antibody (1:5000) for 1 h at RT. The plate was then washed and incubated for 20 min at RT with TMB (50 μL/well). Stop solution for TMB substrate (50 μL/well) was appended to halt the reaction, and the optical density (OD) was measured at 450 nm using a microplate reader.

The contents of LPS in serum or midbrain tissue samples of mice were detected according to the instructions of the manufacturer's instruction. An EnSpire ELISA (PerkinElmer, USA) was used to measure the OD values of each group at 450 nm. The contents of LPS were calculated according to the standard curve.

Transmission electron microscopy

Transmission electron microscopy procedures were conducted as previously described[60]. Briefly, the SN region of the midbrain, with a tissue volume of 1 mm × 1 mm × 1 mm, was rapidly collected and immersed in 2.5% glutaraldehyde at 4 °C for 2–4 h. Subsequently, the tissue was fixed at RT for 2 h using 1% osmium tetroxide in 0.1 M phosphate buffer, followed by three 15-min washes with 0.1 M phosphate buffer. The tissues then underwent sequential dehydration in a graded series of alcohols, with each step lasting 15 min. The specimens were then incubated in a mixture of acetone and embedding resin at ratios of 1:1 for 2–4 h, 2:1 overnight, and pure resin for 5–8 h. Following this, the specimens were incubated overnight in a 37 °C and polymerized for 48 h at 65 °C. Subsequently, sections of 60–80 nm were cut using an ultramicrotome (Leica UC7) and stained in 2% uranium acetate and lead citrate. Finally, samples were examined using a transmission electron microscope (JEM1400PLUS, JEOL, Japan), and images were captured for subsequent analysis.

Statistical analysis

The data were presented as mean values with accompanying standard deviations (SD). One-way analysis of variance (ANOVA) or two-way ANOVA was used for conducting statistical analysis for multiple comparisons. Spearman correlation analysis was used to assess correlations among various experiments, conducted using R. Statistical significance was set at a threshold of $P < 0.05$ to determine statistically significant results.

Data availability

All data generated or analyzed during this study are included in this published article [and its Supplementary Information files].

Received: 9 May 2024; Accepted: 21 February 2025;
Published online: 06 March 2025

References

1. Vijiaratnam, N., Simuni, T., Bandmann, O., Morris, H. R. & Foltynie, T. Progress towards therapies for disease modification in Parkinson's disease. *Lancet Neurol.* **20**, 559–572 (2021).
2. Wang, Q. et al. Post-treatment with an ultra-low dose of NADPH oxidase inhibitor diphenyleneiodonium attenuates disease progression in multiple Parkinson's disease models. *Brain* **138**, 1247–1262 (2015).
3. Chaudhuri, K. R., Healy, D. G. & Schapira, A. H. Non-motor symptoms of Parkinson's disease: diagnosis and management. *Lancet Neurol.* **5**, 235–245 (2006).
4. Vascellari, S. et al. Gut microbiota and metabolome alterations associated with Parkinson's Disease. *mSystems* **5** https://doi.org/10.1128/mSystems.00561-20 (2020).
5. Scheperjans, F. et al. Gut microbiota are related to Parkinson's disease and clinical phenotype. *Mov. Disord.* **30**, 350–358 (2015).
6. Li, W. et al. Structural changes of gut microbiota in Parkinson's disease and its correlation with clinical features. *Sci. China Life Sci.* **60**, 1223–1233 (2017).
7. Munoz-Pinto, M. F. et al. Gut-first Parkinson's disease is encoded by gut dysbiome. *Mol. Neurodegener.* **19**, 78 (2024).
8. Hou, Y. F. et al. Gut microbiota-derived propionate mediates the neuroprotective effect of osteocalcin in a mouse model of Parkinson's disease. *Microbiome* **9**, 34 (2021).
9. Sun, M. F. et al. Neuroprotective effects of fecal microbiota transplantation on MPTP-induced Parkinson's disease mice: gut microbiota, glial reaction and TLR4/TNF-α signaling pathway. *Brain Behav. Immun.* **70**, 48–60 (2018).
10. Round, J. L. & Mazmanian, S. K. The gut microbiota shapes intestinal immune responses during health and disease. *Nat. Rev. Immunol.* **9**, 313–323 (2009).
11. Brudek, T. Inflammatory bowel diseases and Parkinson's disease. *J. Parkinsons Dis.* **9**, S331–s344 (2019).
12. Keshavarzian, A. et al. Colonic bacterial composition in Parkinson's disease. *Mov. Disord.* **30**, 1351–1360 (2015).
13. Romano, S. et al. Meta-analysis of the Parkinson's disease gut microbiome suggests alterations linked to intestinal inflammation. *NPJ Parkinsons Dis.* **7**, 27 (2021).
14. Devos, D. et al. Colonic inflammation in Parkinson's disease. *Neurobiol. Dis.* **50**, 42–48 (2013).
15. Houser, M. C. & Tansey, M. G. The gut-brain axis: is intestinal inflammation a silent driver of Parkinson's disease pathogenesis? *NPJ Parkinsons Dis.* **3**, 3 (2017).
16. Barbara, G. et al. Inflammatory and microbiota-related regulation of the intestinal epithelial barrier. *Front. Nutr.* **8**, 718356 (2021).
17. Cui, C. et al. Curcumin-driven reprogramming of the gut microbiota and metabolome ameliorates motor deficits and neuroinflammation in a mouse model of Parkinson's disease. *Front. Cell. Infect. Microbiol.* **12**, 887407 (2022).
18. Liu, J. et al. Effect of coffee against MPTP-induced motor deficits and neurodegeneration in mice via regulating gut microbiota. *J. Agric. Food Chem.* **70**, 184–195 (2022).
19. Zhang, Y. et al. NLRP3 mediates the neuroprotective effects of SVHRSP derived from scorpion venom in rotenone-induced experimental Parkinson's disease model. *J. Ethnopharmacol.* **312**, 116497 (2023).
20. Li, X. et al. Scorpion venom heat-resistant synthesized peptide ameliorates 6-OHDA-induced neurotoxicity and neuroinflammation: likely role of Na(v) 1.6 inhibition in microglia. *Br. J. Pharmacol.* **178**, 3553–3569 (2021).
21. Qiu, W. et al. Tert-butylhydroquinone attenuates LPS-induced pyroptosis of IPEC-J2 cells via downregulating HMGB1/TLR4/NF-κB axis. *J. Anim. Physiol. Anim. Nutr.* **108**, 194–205 (2024).
22. Gerhardt, S. & Mohajeri, M. H. Changes of colonic bacterial composition in Parkinson's disease and other neurodegenerative diseases. *Nutrients* **10** https://doi.org/10.3390/nu10060708 (2018).
23. Perez-Pardo, P. et al. Gut bacterial composition in a mouse model of Parkinson's disease. *Benef. Microbes* **9**, 799–814 (2018).
24. Zhou, X. et al. The intestinal microbiota exerts a sex-specific influence on neuroinflammation in a Parkinson's disease mouse model. *Neurochem. Int.* **173**, 105661 (2023).
25. Kain, V. et al. Obesogenic diet in aging mice disrupts gut microbe composition and alters neutrophil: lymphocyte ratio, leading to inflamed milieu in acute heart failure. *FASEB J.* **33**, 6456–6469 (2019).
26. Dodiya, H. B. et al. Sex-specific effects of microbiome perturbations on cerebral Aβ amyloidosis and microglia phenotypes. *J. Exp. Med.* **216**, 1542–1560 (2019).
27. Shabani, M., Soti, M., Ranjbar, H. & Naderi, R. Abscisic acid ameliorates motor disabilities in 6-OHDA-induced mice model of Parkinson's disease. *Heliyon* **9**, e18473 (2023).
28. Rafiepour, K., Salehzadeh, A., Bahadori, P., Esmaeili-Mahani, S. & Maneshian, M. Abscisic acid decreases expression of COX-2 and TNF-α proteins in SH-SY5Y neuroblastoma cells as an in vitro model of Parkinson's disease. *Neurosci. Behav. Physiol.* **53**, 688–694 (2023).
29. Özduran, G., Becer, E., Vatansever, H. S. & Yücecan, S. Neuroprotective effects of catechins in an experimental Parkinson's disease model and SK-N-AS cells: evaluation of cell viability, anti-inflammatory and anti-apoptotic effects. *Neurol. Res.* **44**, 511–523 (2022).
30. Angelopoulou, E., Pyrgelis, E. S. & Piperi, C. Neuroprotective potential of chrysin in Parkinson's disease: molecular mechanisms and clinical implications. *Neurochem. Int.* **132**, 104612 (2020).
31. Eisenhofer, G., Kopin, I. J. & Goldstein, D. S. Catecholamine metabolism: a contemporary view with implications for physiology and medicine. *Pharmacol. Rev.* **56**, 331–349 (2004).
32. Jiang, L. et al. A novel role of microglial NADPH oxidase in mediating extra-synaptic function of norepinephrine in regulating brain immune homeostasis. *Glia* **63**, 1057–1072 (2015).
33. Zhong, Z. et al. Fecal microbiota transplantation exerts a protective role in MPTP-induced Parkinson's disease via the TLR4/PI3K/AKT/NF-κB pathway stimulated by α-synuclein. *Neurochem. Res.* **46**, 3050–3058 (2021).
34. Wang, M. et al. Eucommiae cortex polysaccharides attenuate gut microbiota dysbiosis and neuroinflammation in mice exposed to chronic unpredictable mild stress: beneficial in ameliorating depressive-like behaviors. *J. Affect. Disord.* **334**, 278–292 (2023).
35. Guo, T. T. et al. Neuroprotective effects of sodium butyrate by restoring gut microbiota and inhibiting TLR4 signaling in mice with MPTP-induced Parkinson's disease. *Nutrients* **15** https://doi.org/10.3390/nu15040930 (2023).
36. Dong, X. L. et al. Polymannuronic acid prevents dopaminergic neuronal loss via brain-gut-microbiota axis in Parkinson's disease model. *Int. J. Biol. Macromol.* **164**, 994–1005 (2020).
37. Chandran, G. & Muralidhara. Neuroprotective effect of aqueous extract of *Selaginella delicatula* as evidenced by abrogation of rotenone-induced motor deficits, oxidative dysfunctions, and neurotoxicity in mice. *Cell. Mol. Neurobiol.* **33**, 929–942 (2013).
38. Gokul, K. & Muralidhara. Oral supplements of aqueous extract of tomato seeds alleviate motor abnormality, oxidative impairments and neurotoxicity induced by rotenone in mice: relevance to Parkinson's disease. *Neurochem. Res.* **39**, 1382–1394 (2014).

39. García-García, F., Ponce, S., Brown, R., Cussen, V. & Krueger, J. M. Sleep disturbances in the rotenone animal model of Parkinson disease. *Brain Res.* **1042**, 160–168 (2005).
40. Wang, Z. et al. Gut flora metabolism of phosphatidylcholine promotes cardiovascular disease. *Nature* **472**, 57–63 (2011).
41. Yan, J. et al. Gut microbiota induce IGF-1 and promote bone formation and growth. *Proc. Natl. Acad. Sci. USA* **113**, E7554–e7563 (2016).
42. Rakoff-Nahoum, S., Paglino, J., Eslami-Varzaneh, F., Edberg, S. & Medzhitov, R. Recognition of commensal microflora by toll-like receptors is required for intestinal homeostasis. *Cell* **118**, 229–241 (2004).
43. Zhou, Z. L. et al. Neuroprotection of fasting mimicking diet on MPTP-induced Parkinson's disease mice via gut microbiota and metabolites. *NeuroTherapeutics* **16**, 741–760 (2019).
44. Hou, L., Huang, R., Sun, F., Zhang, L. & Wang, Q. NADPH oxidase regulates paraquat and maneb-induced dopaminergic neurodegeneration through ferroptosis. *Toxicology* **417**, 64–73 (2019).
45. Monville, C., Torres, E. M. & Dunnett, S. B. Comparison of incremental and accelerating protocols of the rotarod test for the assessment of motor deficits in the 6-OHDA model. *J. Neurosci. Methods* **158**, 219–223 (2006).
46. Xie, Y. et al. Atractylodes oil alleviates diarrhea-predominant irritable bowel syndrome by regulating intestinal inflammation and intestinal barrier via SCF/c-kit and MLCK/MLC2 pathways. *J. Ethnopharmacol.* **272**, 113925 (2021).
47. Zhao, Z. et al. Fecal microbiota transplantation protects rotenone-induced Parkinson's disease mice via suppressing inflammation mediated by the lipopolysaccharide-TLR4 signaling pathway through the microbiota-gut-brain axis. *Microbiome* **9**, 226 (2021).
48. Perez-Pardo, P. et al. Promising effects of neurorestorative diets on motor, cognitive, and gastrointestinal dysfunction after symptom development in a mouse model of Parkinson's disease. *Front. Aging Neurosci.* **9**, 57 (2017).
49. Turroni, S. et al. Fecal metabolome of the Hadza hunter-gatherers: a host-microbiome integrative view. *Sci. Rep.* **6**, 32826 (2016).
50. Zelena, E. et al. Development of a robust and repeatable UPLC-MS method for the long-term metabolomic study of human serum. *Anal. Chem.* **81**, 1357–1364 (2009).
51. Want, E. J. et al. Global metabolic profiling of animal and human tissues via UPLC-MS. *Nat. Protoc.* **8**, 17–32 (2013).
52. Wang, Q. et al. Locus coeruleus neurons are most sensitive to chronic neuroinflammation-induced neurodegeneration. *Brain Behav. Immun.* **87**, 359–368 (2020).
53. Gao, L. et al. Age-mediated transcriptomic changes in adult mouse substantia nigra. *PLoS ONE* **8**, e62456 (2013).
54. Bucci, D. et al. Systematic morphometry of catecholamine nuclei in the brainstem. *Front. Neuroanat.* **11**, 98 (2017).
55. Zhang, W. et al. Neuroprotective effect of dextromethorphan in the MPTP Parkinson's disease model: role of NADPH oxidase. *FASEB J.* **18**, 589–591 (2004).
56. Hou, L. et al. Paraquat and maneb co-exposure induces noradrenergic locus coeruleus neurodegeneration through NADPH oxidase-mediated microglial activation. *Toxicology* **380**, 1–10 (2017).
57. Wang, Q. et al. Substance P exacerbates dopaminergic neurodegeneration through neurokinin-1 receptor-independent activation of microglial NADPH oxidase. *J. Neurosci.* **34**, 12490–12503 (2014).
58. Song, S. et al. Loss of brain norepinephrine elicits neuroinflammation-mediated oxidative injury and selective caudo-rostral neurodegeneration. *Mol. Neurobiol.* **56**, 2653–2669 (2019).
59. Hou, L., Che, Y., Sun, F. & Wang, Q. Taurine protects noradrenergic locus coeruleus neurons in a mouse Parkinson's disease model by inhibiting microglial M1 polarization. *Amino Acids* **50**, 547–556 (2018).
60. Sun, Q. et al. Clozapine-N-oxide protects dopaminergic neurons against rotenone-induced neurotoxicity by preventing ferritinophagy-mediated ferroptosis. *Free Radic. Biol. Med.* **212**, 384–402 (2024).

Acknowledgements

This study was funded by NSFC-Liaoning Province United Foundation of China (U1908208), Liaoning Province Science and Technology Plan Joint Program (Fund) Project (2023-MSLH-034), Basic Research Projects for the Educational Department of Liaoning Province in 2024 and Dalian Medical University Key planning for Digital Health and Wellness Prescription Inter-disciplinary Research Cooperation Project Team Funding (JCHZ2023002). The funder played no role in the study design, data collection, analysis and interpretation of data, or the writing of this manuscript.

Author contributions

M.C. conducted the experiments, produced, and analyzed the experimental data. Y.Z. performed 16S and metabolomics data analysis, checked and analyzed the experimental data, wrote the manuscript, responded to reviewer comments, and conducted additional experiments. L.H. reviewed and edited the manuscript, and conducted the formal statistical analysis. Z.Z., P.T., and Q.S. assisted with the experiments. J.Z. designed the project, reviewed and edited the manuscript, and provided funding support. Q.W. supervised the project, ensured the reliability of the project results, resolved technical issues during the project, reviewed and edited the manuscript.

Competing interests

The authors declare no competing interests.

Additional information

Supplementary information The online version contains supplementary material available at https://doi.org/10.1038/s41531-025-00892-6.

Correspondence and requests for materials should be addressed to Jie Zhao or Qingshan Wang.